



HETERO-INTERFACES FOR EXTREME ENVIRONMENT ELECTRONICS

Alp Sehirlioglu
CASE WESTERN RESERVE UNIV CLEVELAND OH

07/23/2014
Final Report

DISTRIBUTION A: Distribution approved for public release.

Air Force Research Laboratory
AF Office Of Scientific Research (AFOSR)/ RTB
Arlington, Virginia 22203
Air Force Materiel Command

Report Documentation Page			Form Approved OMB No. 0704-0188		
Public reporting burden for the collection of information is estimated to average 1 hour per response, including the time for reviewing instructions, searching existing data sources, gathering and maintaining the data needed, and completing and reviewing the collection of information. Send comments regarding this burden estimate or any other aspect of this collection of information, including suggestions for reducing this burden, to Washington Headquarters Services, Directorate for Information Operations and Reports, 1215 Jefferson Davis Highway, Suite 1204, Arlington VA 22202-4302. Respondents should be aware that notwithstanding any other provision of law, no person shall be subject to a penalty for failing to comply with a collection of information if it does not display a currently valid OMB control number.					
1. REPORT DATE 14 JUL 2014	2. REPORT TYPE		3. DATES COVERED 15-04-2011 to 14-04-2014		
4. TITLE AND SUBTITLE Hetro-Interefaces For Extreme Electronic Environments			5a. CONTRACT NUMBER		
			5b. GRANT NUMBER		
			5c. PROGRAM ELEMENT NUMBER		
6. AUTHOR(S)			5d. PROJECT NUMBER		
			5e. TASK NUMBER		
			5f. WORK UNIT NUMBER		
7. PERFORMING ORGANIZATION NAME(S) AND ADDRESS(ES) Case Western Reserve University,10900 Euclid Ave,Cleveland ,OH,44106			8. PERFORMING ORGANIZATION REPORT NUMBER		
9. SPONSORING/MONITORING AGENCY NAME(S) AND ADDRESS(ES)			10. SPONSOR/MONITOR'S ACRONYM(S)		
			11. SPONSOR/MONITOR'S REPORT NUMBER(S)		
12. DISTRIBUTION/AVAILABILITY STATEMENT Approved for public release; distribution unlimited					
13. SUPPLEMENTARY NOTES					
14. ABSTRACT					
15. SUBJECT TERMS					
16. SECURITY CLASSIFICATION OF:			17. LIMITATION OF ABSTRACT Same as Report (SAR)	18. NUMBER OF PAGES 23	19a. NAME OF RESPONSIBLE PERSON
a. REPORT unclassified	b. ABSTRACT unclassified	c. THIS PAGE unclassified			

Final Report

HETERO-INTERFACES FOR EXTREME ELECTRONIC ENVIRONMENTS

(AFOSR - FA9550-11-1-0022)

PI: Alp Sehirlioglu

*Department of Materials Science and Engineering, Case Western
Reserve University*

HETERO-INTERFACES FOR EXTREME ELECTRONIC ENVIRONMENTS

Quasi-two-dimensional electron gas (Q-2D-EG) forms at the interface between two perovskite band insulators; LaAlO_3 (LAO) and SrTiO_3 (STO) [1]. Electrical properties of the interface strongly depend on the film thickness [2]. The insulating interface becomes conductive when the film thickness exceeds a critical thickness (3 unit cell for LAO on STO). This conductive interface is two-dimensional in characteristics.

The physical origins of the Q-2D-EG formed at the interface have been under intensive debate to date. Several mechanisms have been proposed, such as the polar catastrophe at the polar LAO/non-polar STO interface [2], structural distortions at the interface [3-5], oxygen vacancies introduced into the LAO/STO hetero-structure during the growth of LAO [1,6,7-9], preferential cationic intermixing at the interface [10-12].

The original hypothesis is of that an intrinsic nature, namely electronic reconstruction at the interface as a result of polar catastrophe forming due to polarization discontinuity. The Q-2D-EG was only observed when films were deposited on Ti-terminated $\langle 001 \rangle$ oriented STO crystals. The $\langle 001 \rangle$ -orientation provides AO – BO₂ stacking in perovskite phase (Fig. 1) [2]. For example, a $\text{SrTiO}_3/\text{LaAlO}_3$ interface normal to $\langle 001 \rangle$ produces a charge-balanced layer of $\text{SrTiO}_3 - (\text{SrO})^0$ or $(\text{TiO}_2)^0$ – intersecting with negatively charged $(\text{AlO}_2)^{1-}$ or positively charged $(\text{LaO})^{1+}$ layers, respectively. (this latter "LaO" layer should not be confused with "LAO", the abbreviation for LaAlO_3). The basic mechanism proposed on the origin of the Q-2D-EG depends on the polarization discontinuity at the interface. This discontinuity results in formation of a dipole between $(\text{AlO}_2)^{1-}$ and $(\text{LaO})^{1+}$ layers; the electrostatic potential increases with increasing thickness

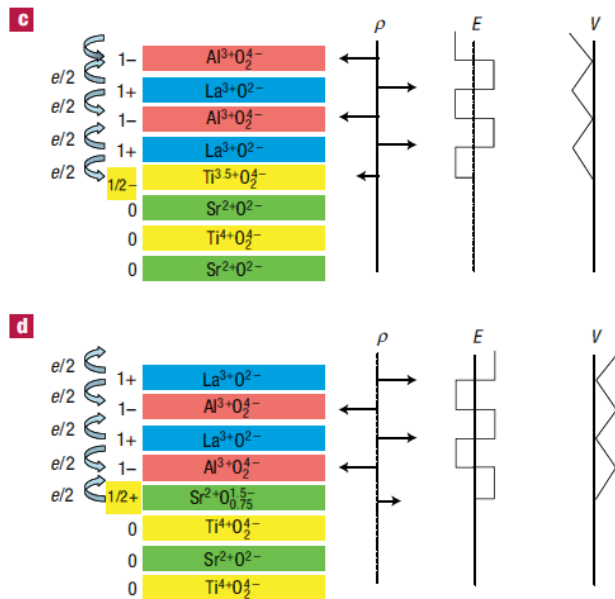


Fig. 1: a) At the $\text{AlO}_2/\text{LaO}/\text{TiO}_2$ interface half an electron is added to the last Ti layer. This produces an interface dipole that causes the electric field (E) to oscillate about 0 and the potential (V) remains finite. The upper free surface is not shown, but in this simple model the uppermost AlO_2 layer would be missing half an electron, which would bring the electric field and potential back to zero at the upper surface. The actual surface reconstruction is more complicated b) The $\text{AlO}_2/\text{SrO}/\text{TiO}_2$ interface has half an electron removed from the SrO plane in the form of oxygen vacancies.[2]

which would result in polar catastrophe. The potential is low when the films are very thin (1-3 unit-cell thick) and the lattice polarization screening allows interface to be insulating. However, the system is not sustainable for thicker films (>3 unit-cell). As the electrostatic voltage increases, the valence band maximum (VBM) at the surface becomes equal to the conduction band minimum (CBM) at the interface, resulting in charge flow from surface to the interface. On a TiO_2 -terminated substrate surface $\text{AlO}_2/\text{LaO}/\text{TiO}_2$ hetero-interface forms; the charge flow from the film surface starts filling up the conduction band Ti 3d states (Fig. 1) [2,9,13]. The polar catastrophe can be eliminated with addition of an electron per two unit cells by changing the valence state of Ti ion from Ti^{4+} to Ti^{3+} . On average at the interface Ti^{4+} becomes $\text{Ti}^{3.5+}$. Unlike semiconductors, at the oxide interface there can be multiple quantum wells; sub-bands of Ti 3d orbitals exist in each of the quantum wells [14,15]. Thus every electron transferred to the Ti3d orbitals may not contribute to conduction. This is also used to describe why the measured charge carrier densities can be lower than what would be expected from the theoretical value of $3.5 \times 10^{-14} \text{ /cm}^2$ (1e- per two unit cells). Orientations with SrO terminated surfaces create $\text{AlO}_2/\text{SrO}/\text{TiO}_2$ interface. The lack of multi-valence states for hole generation – generated by $(\text{AlO}_2)^{1-}$ – results in oxygen vacancy compensation that produces an insulating interface [2,13].

However there have been observations or lack thereof to contradict this hypothesis. For example, no p-type conduction has ever been observed on the surface. As electrons move into the Ti3d bands at the interface, one would expect that holes would form at the valence band, specifically O2p bands on the surface. In addition, below the critical thickness no electrostatic potential build up was observed when investigated by XPS. The electrostatic potential would result in a shift in the valence bands but no such shift has been observed. A third observation that contradicts this intrinsic hypothesis is that Ti^{3+} was observed for films that are thinner than 3 unit cells (below critical thickness). According to the hypothesis, the electron doping of the interface should not have started below critical thickness, thus all Ti should have the 4+ valence state. An intrinsic electronic reconstruction should have the ideal condition when no additional parameters factor in, such as oxygen vacancies (also defined as the extrinsic effect). However, when the films are heated up in oxidizing conditions, the conductivity decreases tremendously as also shown in our results (Figure 2); an unexpected result if the electronic reconstruction was the only mechanism forming the electron gas at the interface.

In general, when the films are deposited at very low partial pressures (below 10^{-5} - 10^{-6} Torr), the charge carrier densities increase to values above the theoretical value, even up to $10^{-16}/\text{cm}^2$. However, at this condition the conductivity is mostly due to oxygen vacancies that form both in the film and the substrate and the conductivity is three dimensional in characteristics. When the deposition is performed at lower vacuum levels (10^{-3} - 10^{-4}), the conductivity is two dimensional in characteristics. No vacancies form in the substrate. However the charge carrier densities are below the theoretical values (Figure 2). As mentioned above one hypothesis is that not all the electrons contribute to electronic contribution but some lay at lower sub-orbitals and stay

localized. Other parameters that can factor in are interfacial strain, intermixing at the interface of A-site cations and B-site cations, cation and anion stoichiometry in the film, surface conditions of the film, specifically redox reaction, and the formation of anti-site defects on the film.

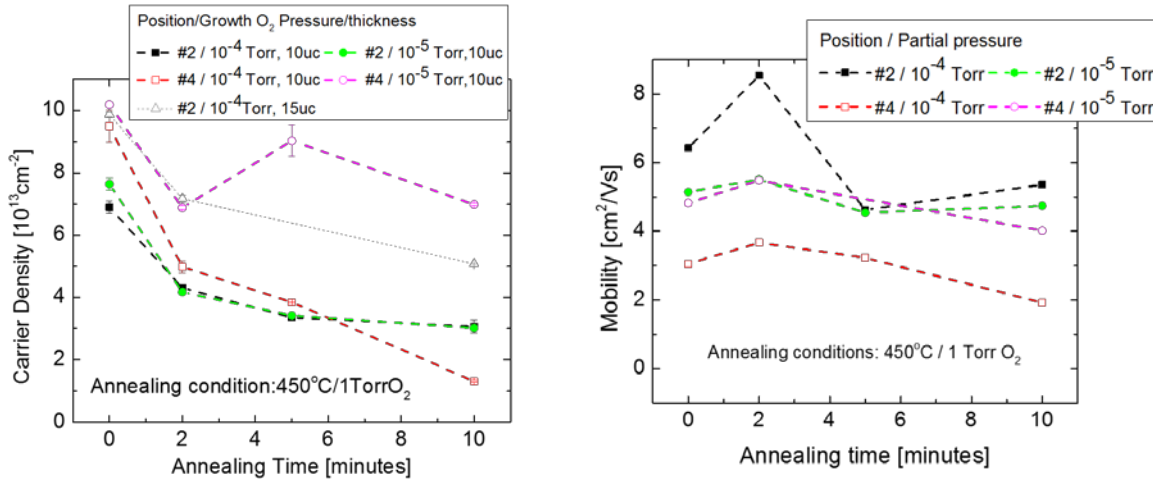


Figure 2: (Left) Charge carrier density of films as a function of annealing time in 1Torr O_2 atmosphere at 450°C . The films are deposited at different partial pressures of oxygen, plume angle and to different thicknesses, as indicated in the legend. (Right) Mobility of the charge carriers for the same films. (Measured at Xuan Gao's laboratories at the Physics Department at Case Western Reserve University).

In 2006, Thiel et al. showed that the interface conductivity was tunable when the film thickness was just below the critical thickness.[6] A conductive atomic force microscopy (AFM) tip was used to apply a positive voltage along the thickness of the film which created a conductive region underneath the tip. This technique allowed writing of conducting wires in between electrodes. Application of a negative voltage converted the interface underneath back into an insulator. The tunability of the interface opened the path for a large number of applications; the focus mostly has been on transistors. The exact origins of the tunability is also still under intensive debate. The electronic reconstruction at the interface requires reconstruction at the surface of the film; structurally, electronically, or chemically. Electronic reconstruction requires holes forming at the surface, however, such p-type surface conduction was never observed. In structural and chemical reconstruction the two most significant factors are: (i) oxygen vacancies and (ii) adsorbed humidity on the surface. Originally, it was suggested that oxygen vacancies at the LAO surface would reduce or completely compensate for the electric field developed in the LAO film; oxygen vacancies contribute electrons to the conduction band – Ti 3d at the interface. The only metallic region in this system is at the $\text{LaAlO}_3/\text{SrTiO}_3$ interface—the surface remains insulating. Tunability of the interface conductivity than can be attained by removing and adding oxygen from and to the surface [16,17]. AFM tip was believed to be able to overcome possible significant kinetic barriers. However, the stability of switching behavior over hundreds of cycles, created doubts about the kinetically burdensome oxygen vacancy mechanisms. In

addition, the interface properties and the stability of the conductive interface were shown to be dependent on storage and test atmospheric conditions [18]. Other suggested mechanisms included adsorbed H_2O which dissociates into OH^- and H^+ adsorbates. Tunability by removing and adding the adsorbates is kinetically more feasible since it does not require physical modification of the oxide hetero-structure [18,19]. Once nano-wires are written they show greater stability under vacuum than regular atmosphere with finite relative humidity. Other suggested mechanisms combine the two factors where the presence of water, changes the kinetics of oxygen vacancy formation [20]. Dissociation of water and attachment of protons on the surface of oxygen atoms can favor formation of oxygen vacancies while the electrons are still free to go to the interface. STO capping of the films allowed circumvention of structural or chemical reconstruction and allowed electronic reconstruction on the surface [21]. As a result, the metallic n-type interface formed at smaller critical thickness (2-unit cells), separated only by $\sim 1\text{nm}$ from an interface with low mobility hole carriers (LAO-STO capping layer interface).

Films were deposited on Ti-terminated crystals. We check the quality of the substrates by measuring the rocking curves as a function of ϕ (Figure 3). A good crystal gives a single domain line with a curvature due to the miscut angle. This crystal then is etched using a buffered hydrofluoric acid (BHF) at $\text{pH}=6$ and then annealed at 900°C . The resulting surface shows terraces with step size of 0.4nm which is approximately equal to that of the STO, 0.3905nm , indicating that the surface was indeed singly terminated (Figure 4). The thickness development of thicker films (7nm - 80nm) and strain development was previously studied by us.[22] The films were shown not to relax ($<4\%$) using reciprocal lattice mapping. Even at greater thicknesses, thus greater stresses due to lattice mismatch, no dislocation formed. Instead, surface cracks formed which resulted in peeling films. Even the remaining parts after peeling were highly strained with negligible relaxation ($<2\%$) (Figure 5). When the thinner films were studied using TEM in collaboration with Marie-Helene Berger (Ecole de Mines, Paris, France), it was shown that the dislocations did not exist in these films as expected. TEM study of 60nm interface length did not show any dislocations (Figure 6). Also the Fourier transformed diffraction patterns showed similar observations to that of reciprocal lattice mapping (which cannot be used for thinner films). The films were pseudomorphic. There was no change in the lattice parameters between the film and the substrate in the in-plane direction (Figure 7).

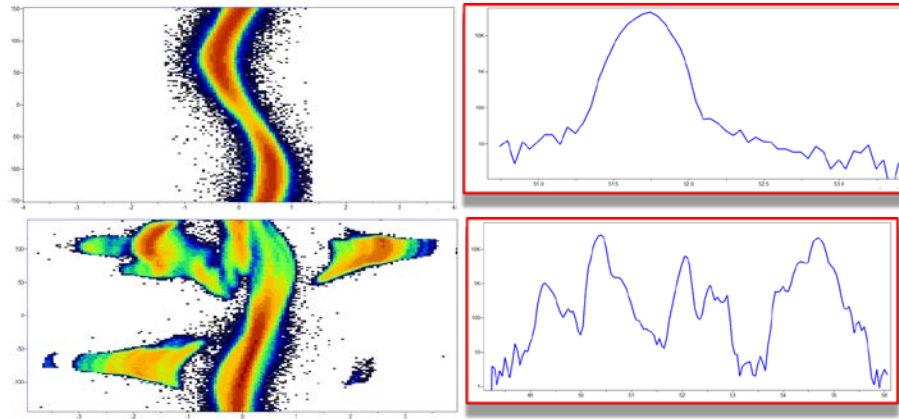


Fig. 3: ϕ - ω plots (left) for two STO substrates from two different vendors. Top crystal is of higher quality with no observable domains. (Right) intensity- ω plots extracted from ϕ - ω plots at around $\phi \approx 100^\circ$, showing the domains clearly for the low quality crystal at the bottom.

The interface properties are strongly influenced by the strain which exists in cube-on-cube growth systems due to lattice mismatch [23]. The epitaxially grown LAO film is strained in LAO/STO heterostructure ($\approx 3\%$ lattice mismatch). The existence of strain field inevitably affects measured electrical properties near the interface, from which the formation of Q-2D-EG at the interface is evidenced. The presence of a critical thickness also indicates that strain in the hetero-epitaxial LAO/STO system may have an effect on the formation of Q-2D-EG[6]. It is also worthwhile pointing out that interfacial strain in a perovskite heterostructure has been shown to alter its physical properties. For example, thin film STO can exhibit strain induced ferroelectricity due to constraints of the substrate [24]. Tensile strain introduced by depositing the STO on substrates with lattice mismatch was shown to eliminate the conductivity at the interface, while increasing compressive stress did not destroy the conductivity but decreased the mobility [25].

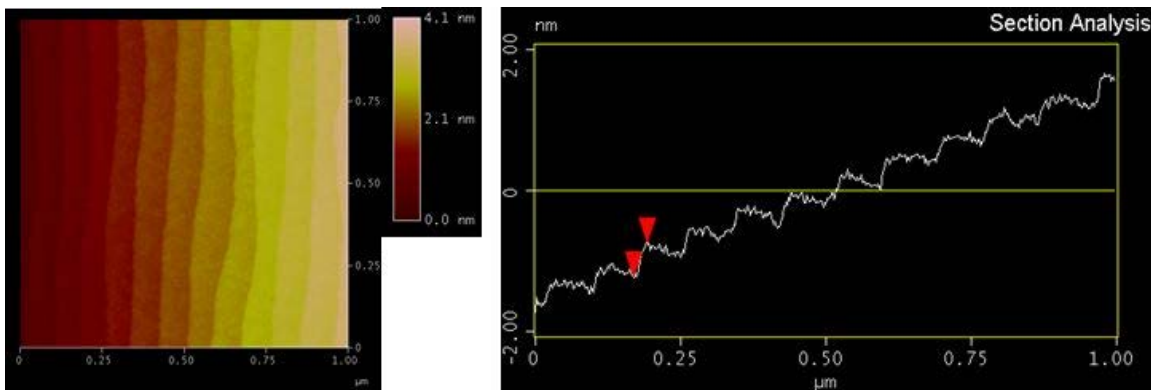


Figure 4: The step size of the terraces is near 4\AA , indicating that the surface was singly terminated.

The origin of the charge at the oxide based heterointerfaces, as well as the factors determining the tunability is under intensive debate to date. There is data that supports all the proposed mechanisms; the theory and modeling efforts trying to unify all the observations resulted in a multitude of conflicting descriptions. Especially quantitative analysis and modeling require a large number of parameters to be investigated. The aforementioned effects are not necessarily exclusive of each other; however, any quantitative analysis would require identification of all the effects on the interface properties.

In general, there is an assumption that the films are stoichiometric in character. Recent work, including original work in this report, suggests that the La/Al ratio is not 1:1 in these films and related defects exist. This non-stoichiometry in general is evidenced to be on the Al-rich side. Our

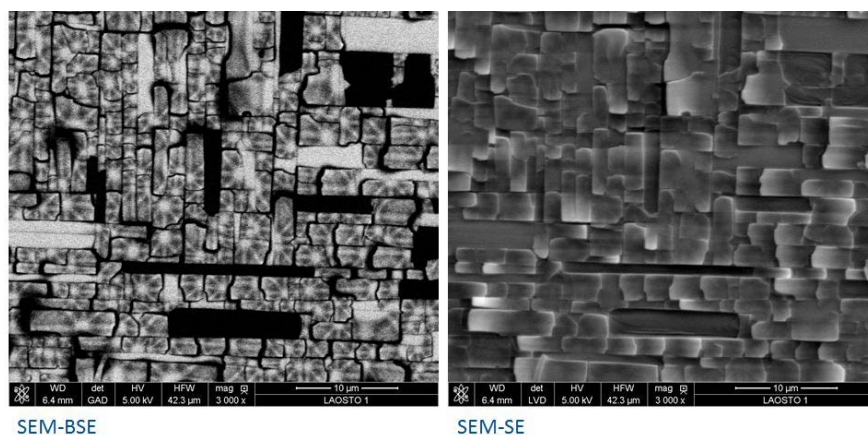


Figure 5: Films peeling off due to increased stress with increasing thickness. The films do not relax.

XPS work shows that decreasing the partial pressure of oxygen during deposition or decreasing the plume angle (Figure 8 and Table I), result in more Al-rich films. Even though the opposite is true, that the La/Al ratio increases with increasing partial pressure of oxygen or increasing plume angle, the films still remain Al-rich and only approach towards unity. To obtain La rich films in PLD it is necessary to go higher partial pressures of deposition (i.e., $>10^{-3}$ Torr) around which the layer-by-layer growth mechanisms may disappear (as observed by RHEED). In characterization of composition with XPS La4d peak is chosen since the kinetic energy is similar to that of Al2p allowing data with similar depth profile. Otherwise Al would have been overrepresented. Composition of the LAO single crystal is verified with ICP and used to calibrate the sensitivity factors for the XPS. Same background and analysis window is used to decrease error in quantification and optimum charge compensation was achieved before every measurement

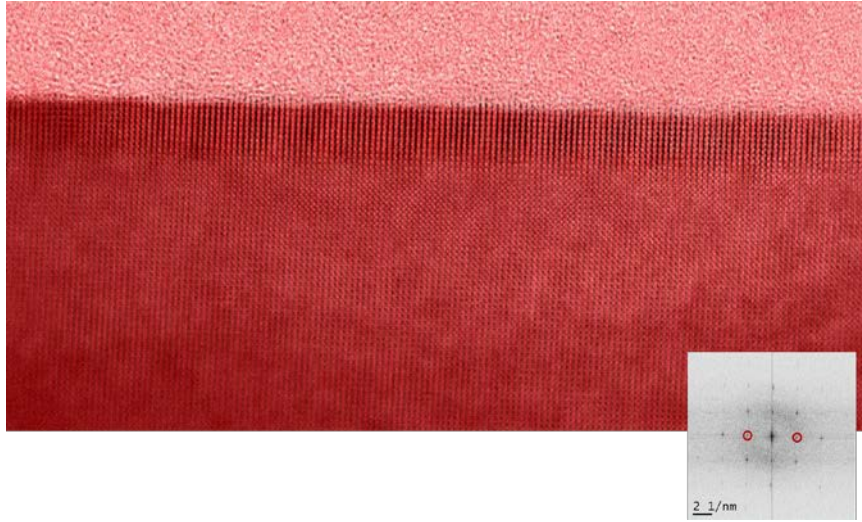
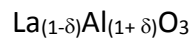


Figure 6: (100) planes continuous across the interface with no dislocations over 60nm. (By our collaborator Marie Helene Berger at Ecole De Mines, Paris, France).

A report using MBE processed films shows that conductivity only forms when the films are Al-rich.[26] The composition is determined in this case with RBS on companion pieces. The extrinsic contributions were ruled out based on the following assumptions: (1) V_o in the STO formed during lower partial pressure growth which was not the case in MBE (2) V_o in the surface region of etched and annealed STO was ruled out since the same crystal was cut into four pieces and were distributed throughout the deposition matrix allowing deposition of La-rich and Al-rich films on the same original single crystal substrate (3) V_o due to bombardment of the STO by energetic species during growth was ruled out based on MBE being a low energy deposition technique (4) chemical mixing of La from LAO into STO was ruled out based on the same discussion for assumption 2, above. The conductivity was only observed in the Al-rich films and the following formulation was provided.



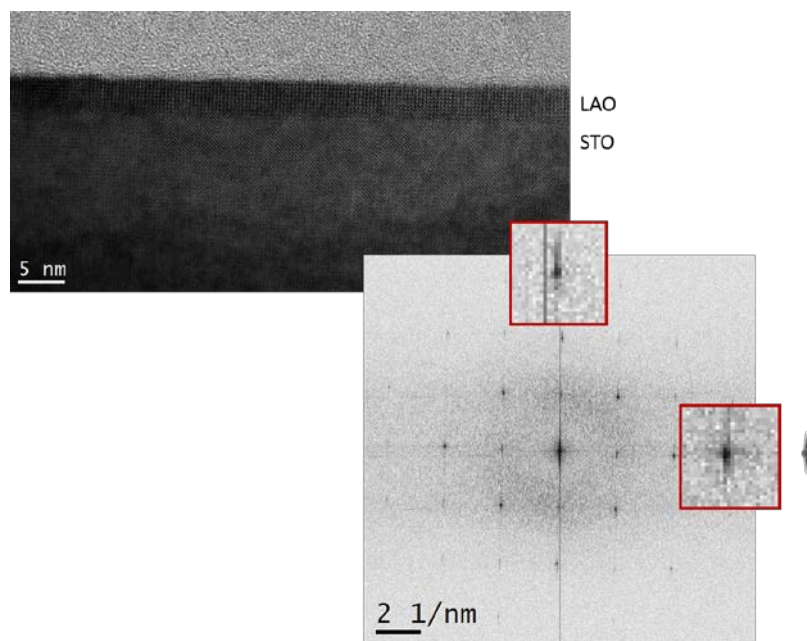


Figure 7: Psuedomorphic films (10 unit cell thick) showing that the relaxation is along the growth direction with no relaxation in in-plane direction.

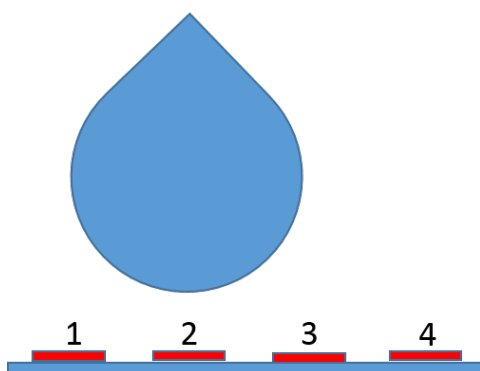


Figure 8: Positions of crystals in relationship to the plume

Table I: Stoichiometry of films as a function of deposition pressure and the plume angle (as described in Figure 8) as measured by XPS.

La/Al		
Single crystal: 1.00		
10 ⁻⁴ Torr	pos. 2: 0.91	pos. 4: 0.94
10 ⁻⁵ Torr	pos. 2: 0.88	

Then for conducting interface to exist the ratio is $(1 - \delta)/(1 + \delta) \leq 0.97 \pm 0.03$ (i.e, Al rich samples are needed). The hypothesis is as follows: When the films are La rich, they cannot occupy any other site then the A-site in the perovskite. Thus La-rich film can form only when Al-vacancies exist at the B-site. As a result, the B-site vacancies can form channels that allow Al-cations to move from the interface to the surface. Such a motion would result in the decrease of the electrostatic potential that build up as a function of thickness and avoid polar catastrophe. As a result, an electron gas won't form at the interface. EELS studies in the same report showed a

greater number of vacancies at the interface for La-rich films in comparison to Al-rich films, consistent with this hypothesis. However, there have not been any observation of such channels yet. In an Al-rich film, since Al can move into A-site, they can form anti-site defects. Thus the polar catastrophe can only be avoided by electronic reconstruction at the interface yielding the electron gas. The argument against why the electron gas does not form in the stoichiometric films is based on local inhomogeneties. It is suggested that every film has inhomogeneties with varying La/Al ratios and in stoichiometric LAO there are enough La-rich regions to form the channels. However, when the $(1-\delta)/(1+\delta) \leq 0.97 \pm 0.03$ is achieved, the La-rich regions become rare enough to not have an effect on the response to polar catastrophe. In bulk LAO, La_{Al} anti-site is costlier than Al_{La} .(27) However, in general anti-sites are higher energy defects than vacancies. However, anti-sites may still form in the films since built-in electric-field can reduce the enthalpy (ΔH) required to form certain defects (until t_c). Thus ground state is not necessarily defect free.

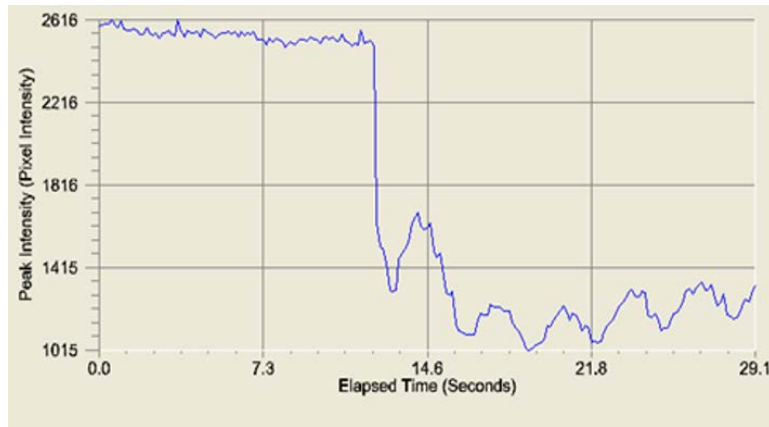


Figure 9: RHEED data showing the fluctuations in the intensity during growth. Each peak corresponds to a layer of film. The noise is due to the pulses. In this case, each peak has 7 noise peaks, corresponding to 7 pulses to form a layer.

Compared to MBE films, our films are deposited with PLD. Thus a higher intermixing is a possibility. Intermixing can also be affected by the plume angle. However, we also divide our crystals into four parts for electrical, compositional and structural analysis, thus obtaining the relationship using the same crystal in single deposition. Films grown at around 10^{-4} Torr provide the two dimensional electron gas with the charge carrier densities in between 10^{13} - $10^{14}/\text{cm}^2$ (Figure 1). TEM studies did not show any V_o formation at the substrate in these deposition conditions. V_o in STO starts forming when the deposition pressure is reduce to 10^{-5} Torr. We verified our thickness using RHEED since the films show layer-by-layer growth characteristics (Figure 9). We were able to obtain large non-stoichiometries as shown in Table I which makes formulation as $\text{La}_{(1-\delta)}\text{AlO}_{3-(3\delta/2)}$ highly improbable. However, the aforementioned formulation

$(\text{La}_{(1-\delta)}\text{Al}_{(1+\delta)}\text{O}_3)$ can be reconfigured to show the site occupancy as follows: $[\text{La}_{(1-\delta)}\text{Al}_{(\delta)}]\text{AlO}_3$. This is an idealized form since there is no-drive to equate $[(\text{Al}-\text{La})/2]/(1-\text{La})=1$. If this equality holds, the excess Al content $(\text{Al}-\text{La})/2$ is equal to the number of La vacancies $(1-\text{La})$, thus all sites are full. However, there can be still additional A-site vacancies that can be charge compensated by V_O . Then the formulation would be: $[\text{La}_{(1-x)}\text{Al}_{(\delta)}\square_{(x-\delta)}]\text{AlO}_{3-[3(x-\delta)/2]}$. This is important because V_{La} forms a deep acceptor state that accepts electrons without conduction and for a 10 unit cell thick film if there are 2% A-site vacancies, the corresponding charge would correspond to half an electron per unit cell, thus it can avoid the polar catastrophe without electronic reconstruction.[28] Also this means that oxygen vacancies can still form in Al-rich films.

In either case Al-rich materials would show Al anti-site defects, thus Al would show a different electrostatic environment in XPS. We have studied in collaboration with AFRL (Dr. Andrei Voevodin) the XPS of these films. A single Gaussian peak was fit successfully to all the peaks despite a variation in La/Al ratio (Table I). The full width half maximum was used as a way of identifying if there is any type of broadening (Figure 10 and Table II). A trend was observed; with increasing Al content the Al-peaks got broader. This is consistent with increasing Al anti-sites with increasing Al content. However, changes are not necessarily statistically significant per the accuracy of the system. A larger data set may help to decrease the statistical uncertainty in these measurements. To decrease the error charging compensation was performed for each system. Also it was shown that no broadening was observed in La, only in Al such broadening was observed. The films studies were 10 unit cell size thick, thus there was no electrostatic potential built-up. In addition, the residual after the peak is on the higher binding energy side. Therefore it cannot be AlO_x .

Table II: The full width half maximum values from Gaussian fits to the Al peaks shown in Figure 10 and the corresponding La/Al ratio showing non-stoichiometry. The values near the titles in each column is the values for the single crystals.

La/Al	1	FWHM (eV)	1.2
0.91	0.94	1.5	1.4
0.88		1.6	

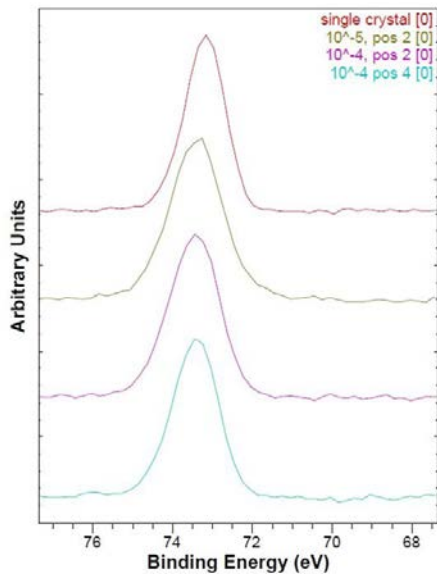


Figure 10: Al 2p peak as observed by XPS.

Diffusion studies were performed on these films using Ar-sputtering with XPS. A gentle Ar sputtering is used to sputter off film layers, then X-rays are used for studying the surface composition. Since the sputtering rate can change from material to material the thickness can only be identified using this technique if some standards are employed. Therefore the composition in general can be plotted as a function of time indicating the time of sputtering. In addition, once the interface is reached, the sputtering can cause intermixing itself. Therefore it is not a good technique to identify the sharpness of the interface. However, the profile can be compared between different cases (i.e., different annealing times etc.) since the contribution of Ar-induced intermixing is expected to be the same in

all conditions. To study the diffusion the films were heated up to temperature at and above deposition temperature and were hold for 10hrs at that temperature. XPS depth profiles (Figure 11) show clearly the pure film and pure substrate regions. The profiles for samples after annealing at 800°C for 10hrs and the as deposited films were the same indicating that at this scale there is no effect of time of exposure on the composition profile. However, when the samples are heated to 1000°C, diffusion of Sr outward was observed. Sr peaks were observed by XPS on the surface of the film. However, no La counter-diffusion was observed. In perovskite structure, there are no interstitial sites for the the A-site cation (i.e., Sr) to diffuse. Therefore the diffusion would need to be substitutional. Since there is no counter diffusion then a regular substitutional diffusion also cannot occur. This type of profile change, then indicated that there are A-site vacancies in the film for Sr to diffuse out without La diffusing in. This is consistent with the above argument and formulation $[La_{(1-x)}Al_{(\delta)}\square_{(x-\delta)}]AlO_{3-3(x-\delta)/2}$ which would mean that both A-site vacancies and oxygen vacancies should exist in the films. However, at this level it is not possible to quantify the content. Increasing A-site vacancy content would indicate a lowering of charge carrier density as discussed previously which may also be the reason why values below theoretical charge carrier densities are observed in general for a two dimensionally conducting system.

When the films are heated to even higher temperatures (1200°C), La starts diffusing in. No B-site cation diffusion is observed at this temperature. Only when the system is heated to 1400°C, we can observe a uniform profile of Sr, La, Al, and Ti in the depth studied. However, when XRD is performed it is possible to see a new peak that is epitaxial. This peak increases in intensity as a

function of annealing time at the expense on LAO peak (Figure 12). This indicates that the film reached a saturation limit of all four cations, however, pristine STO still exists. It is interesting to note that the saturated film is perovskite and keeps its epitaxial relationship. However, the interface sharpness disappears. After exposure for a long time at high temperatures, Sr-diffuses out of the film to form SrO on the surface as observed by SEM (Figure 13).

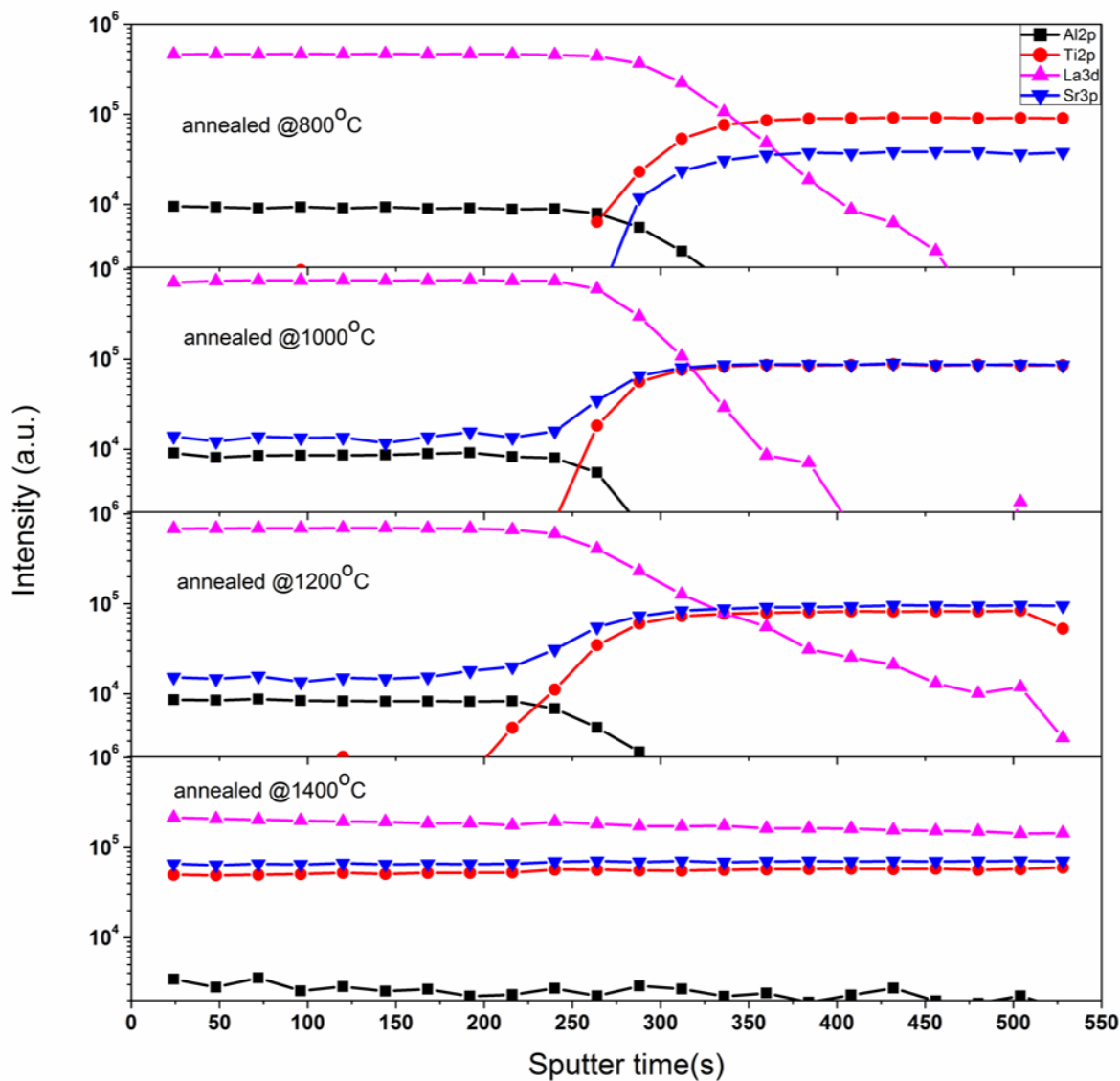


Figure 11: The depth profile using XPS. Cation concentration (in arbitrary units) as a function of sputtering time. Each scan was done after different annealing conditions. The annealing temperatures are reported on each graph and annealing time was 10hrs.

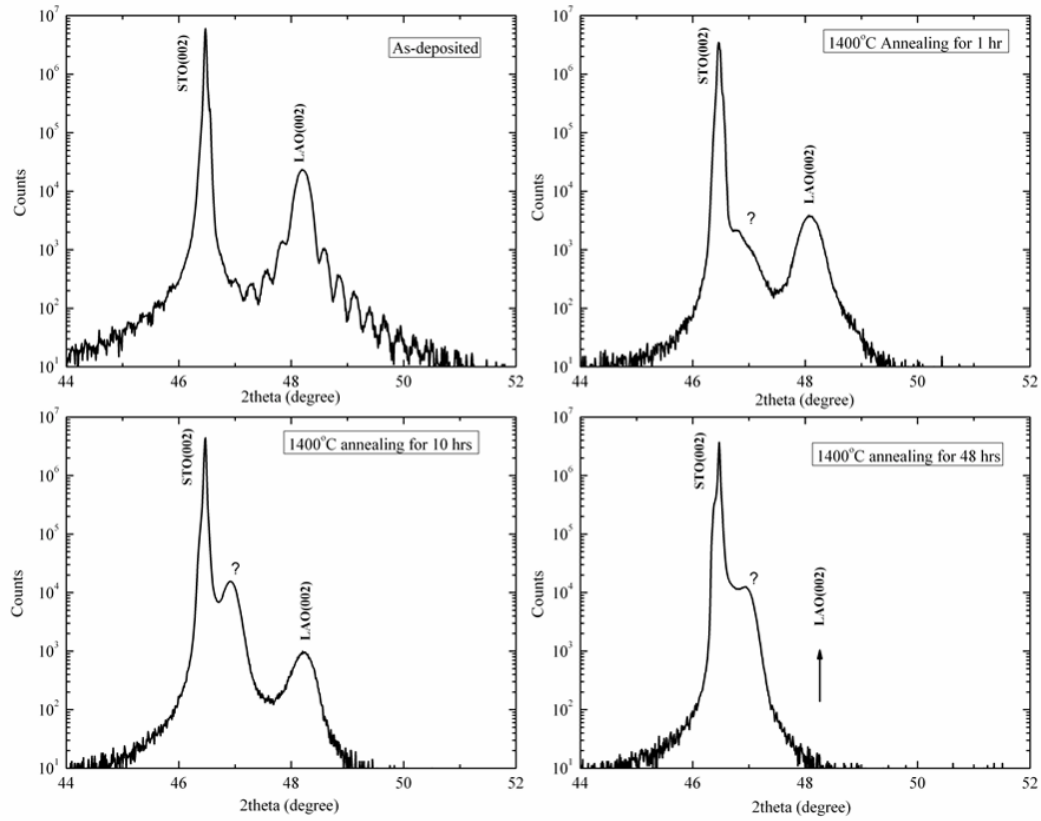


Figure 12: The XRD results after annealing at 1400°C from 1 hour to 48 hours. The extra peak forming in expense of the LAO peak.

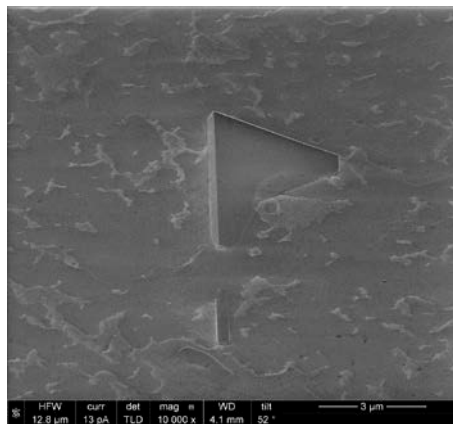


Figure 13: Once the Sr diffuses to the surface, SrO forms on the surface as observed by SEM and EDS.

There is another school of thought describing the intrinsic behavior. In the original intrinsic hypothesis, it was described as the electrostatic field reaching the band gap energy and result in electrons tunneling from the valence band on the surface to the conduction band at the interface. The second thought suggests that the electrons always form no matter the thickness, however when thickness is smaller than the critical thickness, the Fermi energy is above the valence band maximum (VBM) and the electrons flow to the surface.[29] However as the thickness increases, the electrostatic potential brings the VBM above Fermi level and stops electron transfer to the surface. As a result, the two dimensional electron conduction is observed at the interface. In this nuanced approach, the electrons always exist intrinsically but they get trapped at the interface above the critical thickness. Thus the surface conditions and the change in VBM in relationship to Fermi level control the charge carrier density of the 2DEG. For example, oxygen vacancies on the surface result in the formation of the 2DEG but not due to an extrinsic effect, as doping of the electrons, but due to modification of the surface by removal of the oxygen dangling bonds. Thus suppressing the electron transfer to the surface. Higher concentration of oxygen vacancies resemble that of a passivated surface. In such a hypothesis, since the electrons are not originating from the oxygen vacancies, the shallowness or lack thereof of the orbitals does not matter. Therefore, one would expect other types of surface passivation to have a similar effect. As discussed before Hydrogenation of the surface is one of those methods of passivation.[18,19] Hydrogen previously was discussed as donating electrons to the interface but in this hypothesis it functions as a passivator of the surface.

When oxygen leaves an ionically bonded oxide, it leaves as a neutral oxygen gas molecule, thus leaving two electrons behind. Whether these electrons contribute to conduction or not has been discussed earlier at this report. In general, all the electrical measurements were done on films that are exposed to atmospheric air upon removal from the deposition system. Thus, they can have adsorbed species on the surface. The most common one is the $\text{H}_2\text{O}(\text{g})$, that can go through redox reaction on the surface.[28] There are different ways the surface can be modified in the presence of moisture. In an ideal surface with no vacancies H^+ can attach itself to oxygens of the oxide with $1/2\text{O}_2$ leaving to the atmosphere. In this case two electrons per molecule would be donated into the system. In reality there would be oxygen vacancies on the surface (thus $1/2\text{O}_2$ might have left during deposition). In this case, an OH^- can attach itself with Oxygen filling in the vacancy thus creating the same scenario as H attaching itself to the oxygen on the oxide. The other H^+ can attach itself to the oxygen in the oxide. The OH^- attaching itself by filling an oxygen vacancy on the surface (thus by filling a lattice space) will be called lattice-OH. In this case, no $1/2\text{O}_2$ would leave into the surrounding atmosphere. The difference between the two cases can be seen only when comparing the change before and after exposure to moisture. OH^- ions can also attach themselves to surface cations. In this case they are termed advantageous-OH and they are easier to remove in comparison with the lattice-OH.

Study of the oxygen peaks by XPS help us quantify the three types of oxygen in the system. The oxygen forming the oxide (O1s), oxygen filling the lattice site on the surface with a hydrogen attached (lattice-OH) and the advantageous-OH attached to the cations (Figure 14). Measurements were done on 10 unit cell thick samples. Since the formation energy for V_o decreases and the density of surface defects increases with increasing film thickness, the thickness was kept constant. 10 unit cell thickness was also large enough to provide shallow donor states. The room temperature quantified contents of all three types of oxygen for three type of LAO films grown at different deposition atmospheres and the single crystal LAO is shown in Table III. Lattice-OH/O1s main peak area ratio was fixed during this quantification since the systems would need to be heated over 1000°C in UHV to get rid of lattice-OH. Very good fits with this fixed ratio was achieved. Angle resolved XPS (ARXPS) was also performed and the contributions from lattice-OH and advantageous-OH was shown to increase with decreasing angle indicating their location at the surface.

Quantification of the types of oxygen described above showed that the single crystal LAO mostly consists of the oxide oxygen (O1s also observed in deeper parts of the film/substrate) and the advantageous-OH. Thus there were a much lower number of oxygen vacancies in the single crystal, limiting the formation of lattice-OH. This also suggests that the presence of oxygen vacancies promote redox reaction. For the films, no matter what the condition was, the lattice-OH was clearly observed indicating again that the films were oxygen deficient, as discussed before during the part on cation stoichiometry. However, there was not too big of a difference in the lattice-OH content no matter if the deposition pressure was 10^{-4} Torr or 10^{-5} Torr.

Heating the films up to 550°C in UHV of the XPS chamber was enough to evaporate most of the adsorbed advantageous-OH (Figure 15). As described above higher temperatures are needed to evaporate lattice-OH. The content of advantageous-OH decreased from values above 20% for all the samples, including the single crystal, to values below 4% (Table IV). The quantification of lattice-OH vs. advantageous-OH is important since they create different electrostatic

Table III: Three different oxygens identified with peak fitting to O1s peak. The area of peaks (shown in Figure 14) are used to quantify their contribution to the total response for three films deposited at different conditions and the single crystal LAO.

	529.4 eV	530.5 eV	531.4 eV
Sample	<i>oxide</i>	<i>lat.-OH</i>	<i>ad-OH</i>
single crystal	76.5	2.2	21.3
10^{-5} ; pos. 2	56.8	10.7	26.6
10^{-4} ; pos. 2	64.4	10.9	24.7
10^{-4} ; pos. 4	65.3	7.9	26.8

environments on the surface. Lattice-OH acts as a donor where the H donates its electron, while advantageous-OH acts as an acceptor. For example it was shown that the stability of Cu (+) ions on Sapphire is affected whether it was adjacent to advantageous-OH or lattice-OH.[30]

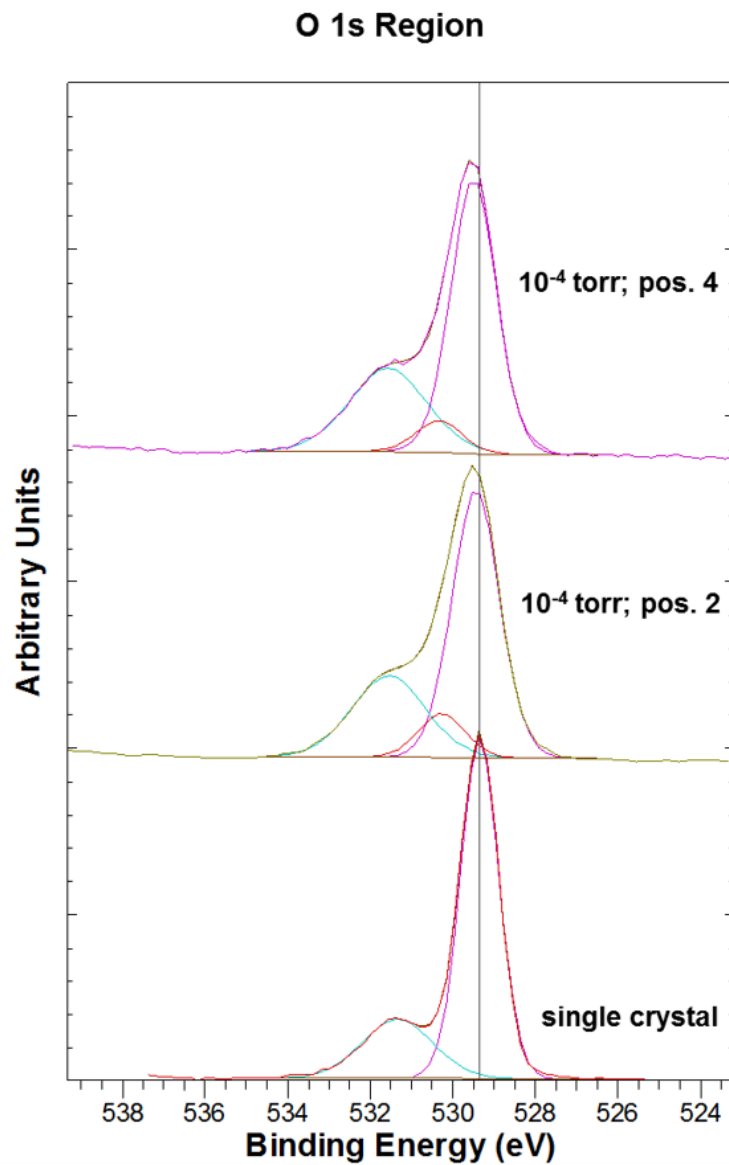


Figure 14: O1s peaks for two films deposited at different conditions and the single crystals LAO. The overlaying result of the fits for three different kinds of oxygen is also shown, as well as the total fit.

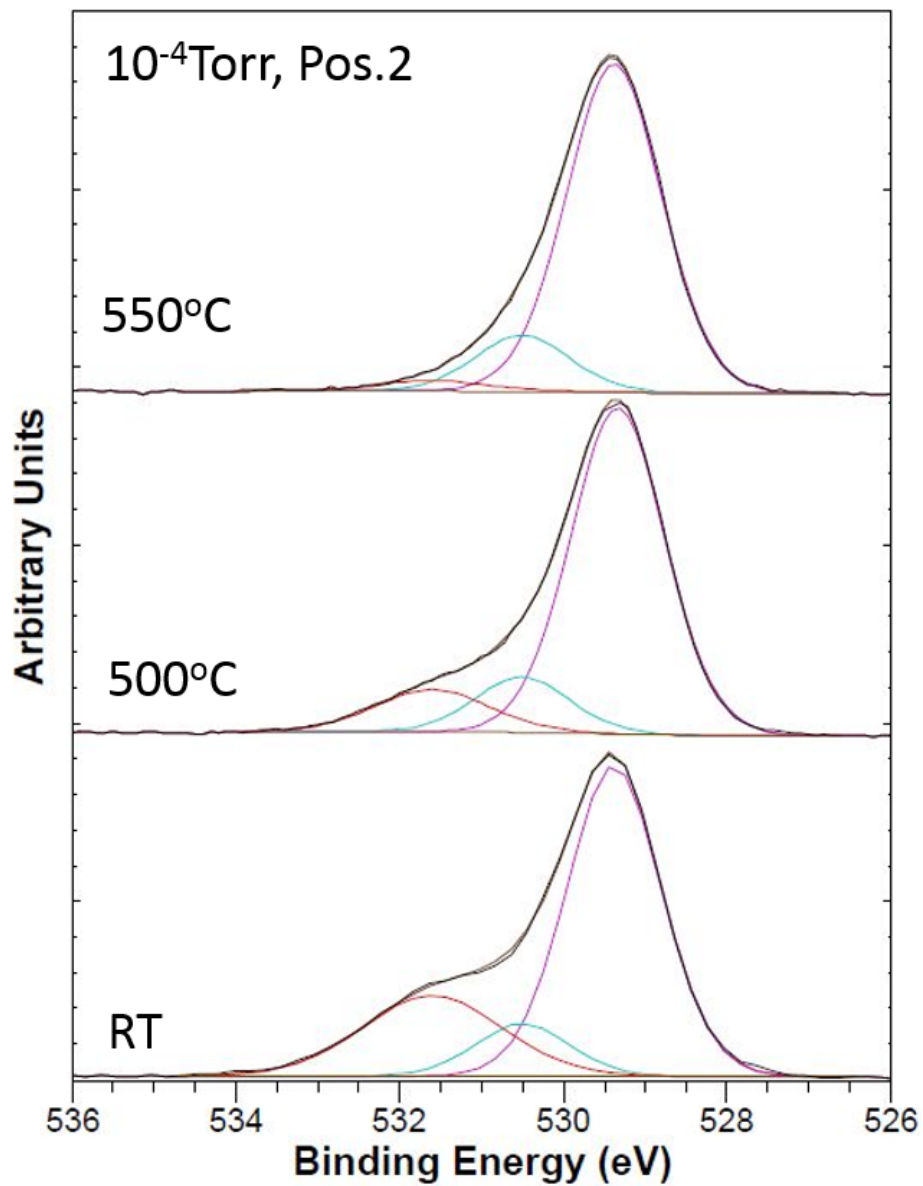


Figure 15: The O1s peak as a function of annealing temperature at UHV of the XPS chamber showing the disappearance of the advantageous-OH. Individual fits for all three types of oxygen is also shown, as well as the total fit. The lattice-OH to oxide-OH ratio was kept constant since the lattice-OH will be stable at these temperatures.

Table IV: The amount of oxide-oxygen, lattice-OH and advantageous-OH (the columns in order) for three films deposited at different conditions and the LAO single crystal after heating up to 550°C in UHV in the XPS chamber.

	550°C		
single crystal	93.5	2.7	3.8
10 ⁻⁵ ; pos. 2	80.9	15.3	3.8
10 ⁻⁴ ; pos. 2	82.9	14.1	3.0
10 ⁻⁴ ; pos. 4	87.1	10.5	2.4

References:

1. A. Ohtomo, and H.Y. Hwang, "A High-Mobility Electron Gas at the LaAlO₃/SrTiO₃ Heterointerface," *Letters to Nature*, **427**, 423 (2004).
2. N. Nakagawa, H. Y. Hwang and D.A. Muller, "Why Some Interfaces Cannot be Sharp," *Nature Materials*, **5**, 204 (2006).
3. S. Okamoto, A.J. Millis, and N.A. Spaldin, "Lattice Relaxation in Oxide Heterostructures: LaTiO₃/SrTiO₃ Superlattices," *Phys. Rev. Lett.*, **97**, 056802 (2006).
4. J.-L. Maurice, C. Carre'te'ro, M.-J. Casanove, K. Bouzehouane, S. Guyard, E. Larquet, and J.-P. Contour, "Electronic conductivity and structural distortion at the interface between insulators SrTiO₃ and LaAlO₃," *Phys. Status Solidi (a)* **203**, 2209 (2006).
5. V. Vonk, M. Huijben, K. J. I. Driessen, P. Tinnemans, A. Brinkman, S. Harkema, and H. Graafsma, "Interface structure of SrTiO₃ /LaAlO₃ at elevated temperatures studied in situ by synchrotron X-rays," *Phys. Rev. B* **75**, 235417 (2007).
6. S. Thiel, G. Hammerl, A. Schmehl, C.W. Schneider, and J. Mannhart, "Tunable Quasi-Two-Dimensional Electron Gases in Oxide Heterostructures," *Science*, **313**, 1942 (2006).
7. R. Pentcheva and W.E. Pickett, "Charge Localization or Itineracy at LaAlO₃/SrTiO₃ Interfaces: Hole Polarons, Oxygen Vacancies, and Mobile Electrons," *Phys. Rev. B*, **74**, 035112 (2006).
8. A. Kalabukhov, R. Gunnarsson, J. Borgesson, E. Olsson, T. Claeson, and D. Winkler, "Effect of Oxygen Vacancies in the SrTiO₃ substrate on the Electrical Properties of the LaAlO₃/SrTiO₃ Interface," *Phys. Rev. B*, **75**, 121404(R) (2007).

9. W. Siemons, G. Koster, H. Yamamoto, W. A. Harrison, G. Lucovsky, T.H. Geballe, D.H.A. Blank, and M.R. Beasley, "Origin of Charge Density at LaAlO₃ on SrTiO₃ Heterointerfaces: Possibility of Intrinsic Doping," *Phys. Rev. Lett.*, **98**, 196802 (2007).
10. P. R. Willmott, S. A. Pauli, R. Herger, C. M. Schlepütz, D. Martoccia, B. D. Patterson, B. Delley, R. Clarke, D. Kumah, C. Cionca and Y. Yacoby, "Structural Basis for the Conducting Interface between LaAlO₃ and SrTiO₃," *Phys. Rev. Lett.*, **99**, 155502 (2007).
11. A. S. Kalabukhov, Yu.A. Boikov, I. T. Serenkov, V. I. Sakharov, V. N. Popok, R. Gunnarsson, J. Borjesson, N. Ljustina, E. Olsson, D. Winkler and T. Claeson, "Cationic Disorder and Phase Segregation in LaAlO₃-SrTiO₃ Heterointerfaces Evidenced," *Phys. Rev. Lett.*, **103**, 146101 (2009).
12. S. A. Chambers, M. H. Engelhard, V. Shutthanandan, Z. Zhu, T. Droubay, L. Qiao, P.V. Sushko, T. Feng, H. D. Lee, T. Gustafsson, E. Garfunkel, A. B. Shah, J. M. Zuo, and Q. M. Ramasse, "Instability, intermixing and electronic structure at the epitaxial LaAlO₃/SrTiO₃ (001) heterojunction," *Surface Science Reports*, **65**, 317 (2010).
13. N. Reyren, S. Thiel, A.D. Caviglia, L.F. Kourkoutis, G. Hammerl, C. Richter, C.W. Schneider, T. Kopp, A.S. Ruetschi, D. Jaccard, M. Gabay, D.A. Muller, J.M. Triscone, and J. Mannhart, "Superconducting Interfaces between Insulating Oxides," *Science*, **317**, 1196 (2007).
14. J. Mannhart and D.G. Schlom, "Oxide Interfaces-An Opportunity for Electronics," *Science* **327**, 1607 (2010).
15. R. Arras, V.G. Ruiz, W.E. Pickett, R. Pentcheva, "Tuning the two-dimensional electron gas at the LaAlO₃/SrTiO₃ (001) interface by metallic contacts," *Phys. Rev. B* **85**, 125404 (2012).
16. C. Cen, S. Thiel, G. Hammerl, C.W. Schineider, K.E. Andersen, C.S. Hellberg, J. Mannhart, and J. Levy, "Nanoscale control of an interfacial metal-insulator transition at room temperature," *Nature Materials*, **7**, 298 (2008).
17. Y.Z. Chen, J.L. Zhao, J.R. Sun, N. Pryds, and B.G. Shen, "Resistance switching at the interface of LaAlO₃/SrTiO₃," *Appl. Phys. Lett.* **97**, 123102 (2010).
18. F. Bi, D. F. Bogorin, C. Cen, C.W. Bark, J.W. Park, C-B. Eom, and J. Levy, "Water cycle mechanism for writing and erasing nanostructures at the LaAlO₃/SrTiO₃ interface", *Appl. Phys. Lett.* **97**, 173110 (2010).
19. W-J. Son, E. Cho, J. Lee, and S. Han, "Hydrogen adsorption and carrier generation in the LaAlO₃-SrTiO₃ heterointerfaces: a first principles study," *J. Phys.: Condens. Matter* **22**, 315501 (2010).
20. N.C. Bristowe, P.B. Littlewood, and E. Artacho, "Surface defects and conduction in polar oxide heterostructures," *Phys. Rev. B* **83**, 205405 (2011).
21. R. Pentcheva, M. Huijben, K. Otte, W.E. Pickett, J.E. Kleibeuker, J. Huijben, H. Boschker, D. Kockmann, W. Simeons, G. Koster, H.J.W. Zandvliet, G. Rijnders, D.H.A. Blank, H. Hilgenkamp, and A. Brinkman, "Parallel Electron-Hole Bilayer Conductivity from Electronic Interface Reconstruction," *Phys. Rev. Lett.* **104**, 166804 (2010).
22. W. Wei and A. Sehirlioglu, "Strain relaxation analysis of LaAlO₃/SrTiO₃ heterostructure using reciprocal lattice mapping," *Appl. Phys. Lett.*, **100**, 071901 (2012).
23. W. Nix, *Metall. Mater. Trans. A*, **20**, 2217 (1989).
24. J. H. Haeni, P. Irvin, W. Chang, R. Uecker, P. Reiche, Y. L. Li, S. Choudhury, W. Tian, M. E. Hawley, B. Craigo, A. K. Tagantsev, X. Q. Pan, S. K. Streiffer, L. Q. Chen, S. W. Kirchoefer, J. Levy, and D. G. Schlom, "Room-temperature ferroelectricity in strained SrTiO₃," *Nature*, **430**, 758 (2004).

25. Tailoring a two-dimensional electron gas at the LaAlO₃/SrTiO₃ (001) interface by epitaxial strain, C. W. Bark, D. A. Felker, Y. Wang, Y. Zhang, H. W. Jang, C. M. Folkman, J. W. Park, S. H. Baek, H. Zhou, D. D. Fong, X. Q. Pan, E. Y. Tsybal, M. S. Rzchowski, and C. B. Eoma, *Proc. Natl. Acad. Sci.* **108**, 4720-4724(2011).
26. M.P. Warusawithana; C. Richter; J.A. Mundy; P. Roy; J. Ludwig; S. Paetel; T. Heeg; A.A. Pawlicki; L.F. Kourkoutis; M. Zheng; M. Lee; B. Mulcahy; W. Zander; Y. Zhu; J. Schubert; J.N. Eckstein; D.A. Muller; C.S. Hellberg; J. Mannhart; D.G. Schlom, "LaAlO₃ stoichiometry is key to electron liquid formation at LaAlO₃/SrTiO₃ interfaces," *Nature Comm*, **4**, 2351 (2013).
27. M. Choi, A. Janotti, and C. G. Van de Walle, "Native point defects in LaAlO₃: A hybrid functional study", *Phys. Rev. B* **88**, 214117 (2013).
28. N.C. Bristowe, P. Ghosez, P.B. Littlewood and E. Artacho, "The origin of two-dimensional electron gases at oxide interfaces: insights from theory", *J. Phys.: Condens. Matter* **26**, 143201 (2014).
29. A. Janotti, L. Bjaalie, L. Gordon, and C.G. Van de Walle, "Controlling the density of the two-dimensional electron gas at the SrTiO₃/LaAlO₃ interface," *Phys. Rev. B.* **86**, 241108(R) (2012)
30. C. Niu; K. Shepherd; D. Martini; J. Tong; J.A. Kelber; D.R. Jennison; A. Bogicevic, "Cu interactions with α -Al₂O₃(0001): effects of surface hydroxyl groups versus dehydroxylation by Ar-ion sputtering," *Surf. Sci.* **465** [1–2], 163 (2000).